Ethanol-assisted ablation of silicon and germanium by temporally shaped femtosecond pulses

Guangming Zhang (张广鸣)[1], Xin Li (李 欣)[1,*], Lan Jiang (姜 澜)[1], Xuesong Shi (史雪松)[1], Kaihu Zhang (张开虎)[1], Qiang Cao (曹 强)[1], and Yongfeng Lu (陆永枫)[2]

[1]*Laser Micro/Nano Fabrication Laboratory, School of Mechanical Engineering, Beijing Institute of Technology, Beijing 100081, China*

[2]*Department of Electrical Engineering, University of Nebraska-Lincoln, Lincoln, Nebraska 68588-0511, USA*

**Corresponding author: lixin02@bit.edu.cn*

Received December 5, 2014; accepted January 16, 2015; posted online March 10, 2015

A surprising phenomenon can be discovered by using femtosecond double-pulse ablation of silicon and germanium in ethanol. The ablation areas present an oscillation increase phenomenon when the pulse delay increases from 200 fs to 1 ps in the fluence range of 0.5–0.6 J/cm^2. In contrast, the ablation areas exhibit an oscillation decrease phenomenon as the pulse delay increases when the laser fluence $F < 0.5$ J/cm^2, which is consistent with the results of the experiment in air. It is considered that the adjustment of the photon–electron coupling efficiency by pulse train technology plays an important role in the ablation process.

OCIS codes: 140.3390, 320.5540, 320.2250.
doi: 10.3788/COL201513.041402.

In recent years, the femtosecond (fs) laser has attracted extensive attention in micro/nano-fabrication as a promising tool, as it can offer the capability of non-thermal processing due to its ultra-short pulse durations and ultra-high power densities[1–3]. Compared to ablation in ambient air, liquid-assisted ablation of materials by fs laser pulses has proved to be an efficient tool for a variety of highly precise fabrications[4–6]. The presence of liquid easily reduces the laser-induced residual thermal damages and removes the debris re-deposition. For example, Shaheen *et al.* obtained cleaner surfaces and less debris re-deposition when they used a fs laser to ablate the brass in water and ethanol, compared to their ablation results in ambient air[7]. Daminelli *et al.* investigated the fs laser single-pulse interaction with silicon (Si) underwater, and demonstrated that a difference in morphological characteristics between the laser-induced craters produced in water and air is obtained[8].

The ablation characteristics of fs double pulses with pulse delay ranging from several fs to several hundred picoseconds and their interaction with many different materials have attracted considerable attentions in the past decades[9–17]. Kim *et al.* found a decrease in the ablation area when the values of the pulse delays are in picoseconds[9]. Similarly, Povarnitsyn *et al.* investigated the suppression of the ablation depth in the crater that occurs when there is a long delay[13]. In our previous experiments, we discovered the quasiperiodic oscillation of the ablation areas in semiconductors by using fs double pulses with pulse delays in fs in ambient air[14]. Compared with the conventional laser, the fs double-pulse laser makes it possible to adjust the localized electron density and energy coupling, which has been shown to be advantageous in laser machining[16].

In this Letter, the ablation areas on Si for fs double-pulse delays ranging from 0 to 1 ps in air and ethanol are measured. Different oscillation phenomena of the ablation areas are observed with an increase in pulse delays within several hundred fs under different laser fluences in ethanol. An abrupt increase in the ablation areas at the delay time of 200 fs is observed in ethanol when the laser fluence exceeds 0.4 J/cm^2. Through atomic force microscope (AFM) images, we discovered that a better surface quality and deeper ablation depth of the crater is obtained at a delay time of 500 fs in ethanol, compared to the crater ablated by the conventional laser in air. A similar phenomenon is also found during the fs double-pulse ablation of germanium (Ge) in ethanol.

In the experiments, the laser source is a Ti:sapphire laser regenerative amplifier system, which delivered 50 fs pulses of linearly polarized light at a central wavelength of 800 nm. The temporal pulse shaping is conducted by a 4f pulse shaper (Biophotonic Solutions Inc., MIIPSBOX 640), which can shape a fs pulse into double fs pulses with the same energy distribution and can change the delay time from 0 to 4.0 ps. The laser pulses are focused on the target via a 100× plano-convex lens with a focal length of 100 mm. A CCD camera is used to observe the ablation process. The fluences F (averaged value over the laser beam cross section) of the pulses are measured in front of the objective lens. An electromechanical shutter is used to control the number of laser pulses. In the liquid experiments, the thickness of the liquid layer above the sample surface is about 3 mm. The samples are stuck to the bottom of a glass vessel that is mounted on a computer-controlled six-axis motion stage (M-840.5DG, PI, Inc.) with a positioning resolution of 1 μm. Considering the different focal conditions in the different ambiences, the same

focal positions are obtained by moving the sample along the optical axis. The crystal orientations of the Si and Ge all are ⟨111⟩, and the optically polished samples have a thickness of 1 mm. All experiments are carried out at room temperature.

Figure 1 shows the scanning electron microscope (SEM) images of the crater morphologies obtained by fs laser ablation of Si in air and ethanol at the pulse delay times (Δt) of 0, 200, 500, and 1000 fs. Figure 1(a) shows the SEM images of the ablation craters obtained at the total laser fluence of 0.6 J/cm^2, which is higher than the 20-shots ablation threshold of 0.31 J/cm^2 measured in our experiments. The repetition rate is 20 Hz. In the air experiments, fs laser-induced periodic surface structures are observed in the fringe areas of the craters in Fig. 1(a). At $\Delta t = 0$ fs, as shown in Fig. 1(a), the ablation area is about 481.1 μm^2. At $\Delta t = 200$ fs, the ablation area decreases to 357.8 μm^2. At $\Delta t = 500$ fs, the ablation area increases to 360.5 μm^2, and then decreases to 331.5 μm^2 at the pulse delay of 1000 fs. Hence, the areas of the ablated craters obtained in air when $\Delta t > 0$ fs are less than the crater obtained by the conventional single pulse ($\Delta t = 0$ fs). For ethanol-mediated irradiation at the laser fluence of 0.4 J/cm^2, as shown in Fig. 1(b), the areas of the ablated crates are 303.1, 237.6, 211.1, and 198.5 μm^2, which correspond to the time of the pulse delays $\Delta t = 0$, 200, 500, and 1000 fs. A similar phenomenon is presented with the experiments in the air. Figure 1(c) shows the SEM images of the ablation craters at the laser fluence of 0.6 J/cm^2. At $\Delta t = 0$ fs, the ablation area is 325.1 μm^2. At $\Delta t = 200$ fs, the ablation area abruptly increases to 388.6 μm^2. At $\Delta t = 500$ fs, the ablation area increases to 402.7 μm^2, and then decreases to 364.6 μm^2 at the pulse delay of 1000 fs. Compared to the conventional single pulse, the phenomenon of the enhanced ethanol-mediated ablation is different with the ablation experiments in air, which present an ablation increase trend when $\Delta t > 200$ fs.

In order to further research the trend of the average ablation areas as the function of pulse delays during fs double-pulse ablation of Si in air and ethanol, we used 20 pulses at a 20 Hz repetition rate on the target, with the laser fluence ranging from 0.3 to 0.6 J/cm^2 (Fig. 2). As shown in Fig. 2(a), the ablation areas present a quasiperiodic oscillation decrease phenomenon with the increase of the pulse delay in air, which is consistent with our previous experimental results[14]. It implies that the oscillation of the atomic motion caused by the carrier density changes leads to quasiperiodic variations in the ablation area. The fs double pulses significantly influence the carrier density. Hence, the oscillation of the atomic motion can be adjusted by changing the delay of the fs double pulse[14]. Figure 2(b) shows the ablation areas as a function of the pulse delays under the same experimental conditions, but in ethanol. Two different variation rules for the ablation areas are observed under different fluence ranges. Compared to the ablation in the air, the same experimental phenomena can be found when the laser fluence is less than 0.5 J/cm^2. However, when the laser fluence increases from 0.5 to 0.6 J/cm^2, the ablation areas present an oscillation increase phenomenon with an increase in the pulse delay. As shown in Fig. 2(b), the ablation areas of the ablated craters abruptly increase from 200 fs to 1 ps.

The morphologies of craters ablated in air are different from those ablated in ethanol. Figure 3(a) shows the center image of the ablated crater in air after twenty pulses of radiation at $F = 0.6$ J/cm^2 with the delay time of 500 fs. One can clearly see that the grooves' structure has a trace of melting in the center image of the laser-irradiated spot. A rippled structure is also found in the

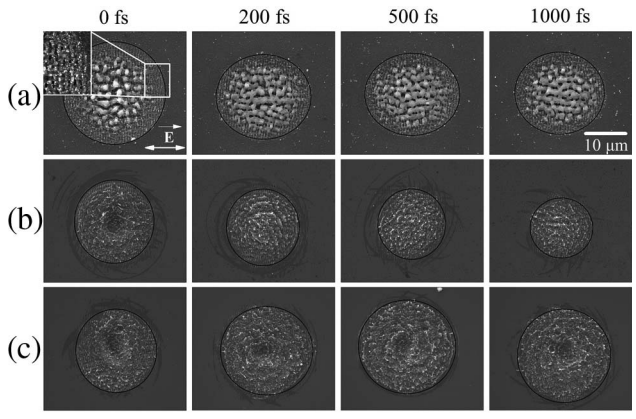

Fig. 1. SEM images of craters produced by 20 double pulses at a repetition rate of 20 Hz in different mediums: (a) in air, $F = 0.6$ J/cm^2; (b) in ethanol, $F = 0.4$ J/cm^2; (c) in ethanol, $F = 0.6$ J/cm^2.

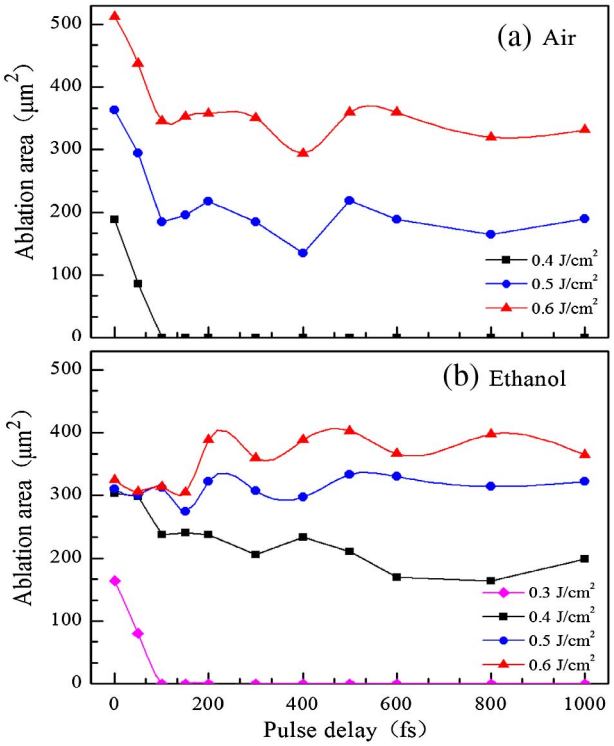

Fig. 2. Ablation area as a function of the pulse delays at different laser fluences: (a) air, (b) ethanol.

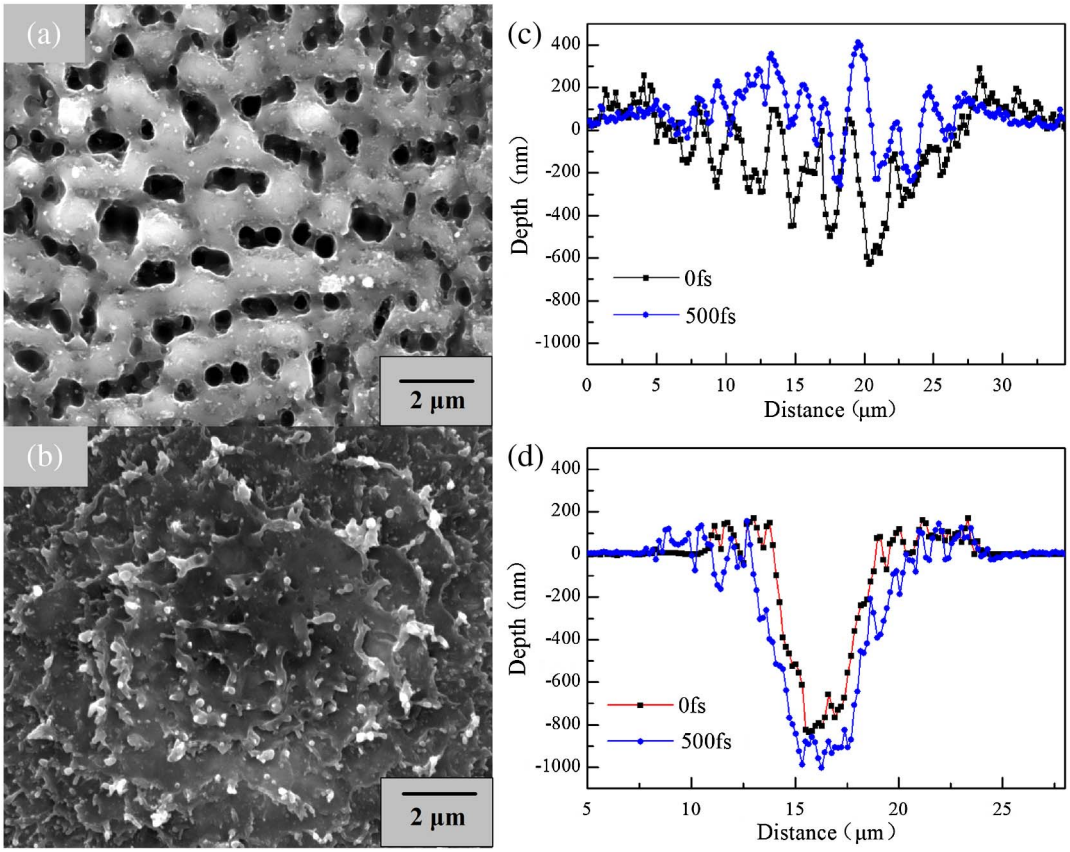

Fig. 3. SEM images of crater morphologies obtained at $\Delta t = 500$ fs in (a) air and (b) ethanol. Two-dimensional profiles of the craters produced in (c) air and (d) ethanol.

annular region around the center of the craters[18], as shown in Fig. 1(a). For the ethanol-mediated irradiation, fold-shaped structures appeared as radially oriented narrow fronts over the ablation areas. This is caused by the interaction of the fs laser with Si in ethanol, and can be seen in Fig. 3(b). The formation of the morphology is attributed to the liquid-related effects induced by the incident laser interaction with the ethanol solution[5,19]. Furthermore, a better surface quality can be obtained around the craters in ethanol. The presence of the liquid could reduce the formation of re-solidified molten material and take away the debris in the ethanol solution[20,21]. The two-dimensional profiles obtained by AFM measurement of the craters produced in air and ethanol is shown in Figs. 3(c) and 3(d). As shown in Fig. 3(c), the depth of the crater obtained at a single pulse in air is deeper than the depth obtained at $\Delta t = 500$ fs. However, compared to the single pulse in ethanol, a deeper crater is obtained at the delay time of 500 fs, which is the opposite of the result in air.

The aforementioned experimental results show the influences of the pulse shaping at different laser fluences on the ablation areas, which may be attributed to the adjustment of the photon–electron coupling efficiency by pulse train technology[22]. When the laser fluence exceeds 0.4 J/cm^2, the photon absorption efficiency maybe enhanced due to the change in the free electron density as the pulse delay increases. The generation of electrons by the photoionization of ethanol molecules can occur as fast as ~200 fs, due to the separation of hydrogen bonds[23,24]. Hence, the free electron density falls back around the critical density when the pulse separation $\Delta t > 200$ fs[4]. A higher photon–electron coupling efficiency is obtained at $\Delta t > 200$ fs when the second sub-pulse arrives.

A similar phenomenon in the ablation characteristics is also observed in Ge when the fs double pulse ablates the

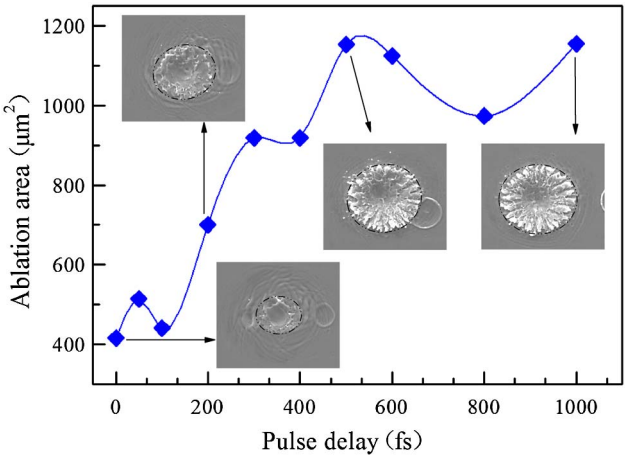

Fig. 4. Ablation area as a function of pulse delays in Ge in the ethanol solution.

target in ethanol at a laser fluence of 0.6 J/cm^2. As shown in Fig. 4, the ablated craters with fold-shaped structures are found when the pulse delay in ethanol is $\Delta t > 200$ fs. This is consistent with the ablation experiments with Si.

In conclusion, different ablation characteristics are discovered when Si is ablated in air and ethanol using fs double-pulse ablation. Compared to the oscillation decrease phenomenon of the ablation areas in air, an oscillation increase phenomenon of the ablation areas in ethanol is found when the fs laser fluence exceeds 0.4 J/cm^2. Different surface structures are obtained in different mediums, and the AFM images show that the ablation rate is higher in ethanol as the pulse delay increases. It is assumed that the unexpected ablation characteristics are due to the increase of the photon absorption efficiency, which is achieved by adjusting the free electron density during the fs double-pulse ablation in ethanol. In addition, a similar phenomenon of the ablation areas as a function of the pulse delays is also obtained at a particular laser fluence by using fs double-pulse ablation of Ge in ethanol.

This work was supported by the National Basic Research Program of China (973 Program) (Grant No. 2011CB013000) and the National Natural Science Foundation of China (NSFC) (Grant Nos. 91323301and 51375051).

References

1. R. R. Gattass and E. Mazur, Nat. Photonics **2**, 219 (2008).
2. M. E. Povarnitsyn, T. E. Itina, M. Sentis, K. V. Khishchenko, and P. R. Levashov, Phys. Rev. B **75**, 235414 (2007).
3. J. Wang and C. Guo, Appl. Phys. Lett. **87**, 251914 (2005).
4. N. Leng, L. Jiang, X. Li, C. C. Xu, P. J. Liu, and Y. F. Lu, Appl Phys A **679**, 109 (2012).
5. S. Bashir, H. Vaheed, and K. Mahmood, Appl. Phys. A **389**, 110 (2013).
6. Y. Ju, C. Liu, Y. Liao, Y. Liu, L. Zhang, Y. Shen, D. Chen, and Y. Cheng, Chin. Opt. Lett. **11**, 072201 (2013).
7. M. E. Shaheen, J. E. Gagnon, and B. J. Fryer, J. Appl. Phys **113**, 213106 (2013).
8. G. Daminelli, J. Krüger, and W. Kautek, Thin Solid Films **334**, 467 (2004).
9. J. Kim, S. Na, S. Cho, W. Chang, and K. Whang, Opt. Lasers Eng. **46**, 306 (2008).
10. T. J.-Y. Derrien, J. Krüger, T. E. Itina, S. Höhm, A. Rosenfeld, and J. Bonse, Opt. Express **21**, 29643 (2013).
11. L. Jiang and H. L. Tsai, Appl. Phys. Lett. **87**, 151104 (2005).
12. J. Bonse, J. Krüger, S. Höhm, and A. Rosenfeld, J. Laser Appl. **24**, 042006 (2012).
13. M. E. Povarnitsyn, T. E. Itina, K. V. Khishchenko, and P. R. Levashov, Phys. Rev. Lett. **103**, 195002 (2009).
14. X. Li, C. Li, L. Jiang, X. S. Shi, N. Zhang, and Y. F. Lu, Opt. Lett. **39**, 2382 (2014).
15. M. Barberoglou, D. Gray, E. Magoulakis, C. Fotakis, P. A. Loukakos, and E. Stratakis, Opt. Express **21**, 18501 (2013).
16. R. Stoian, M. Boyle, A. Thoss, A. Rosenfeld, G. Korn, I. V. Hertel, and E. E. B. Campbell, Appl. Phys. Lett. **80**, 353 (2002).
17. C. Xu, L. Jiang, N. Leng, Y. Yuan, P. Liu, C. Wang, and Y. Lu, Chin. Opt. Lett. **11**, 041403 (2013).
18. J. Bonse and J. Krüger, J. Appl. Phys **108**, 034903 (2010).
19. H. Bian, Q. Yang, H. W. Liu, F. Chen, G. Q. Du, J. H. Si, and X. Hou, Mater. Sci. Eng. C **33**, 663 (2013).
20. H. W. Liu, F. Chen, X. H. Wang, Q. Y. Yang, H. Bian, J. H. Si, and X. Hou, Thin Solid Films **518**, 5188 (2010).
21. J. F. Herbstman, A. J. Hunt, and S. M. Yalisove, Appl. Phys. Lett. **93**, 011112 (2008).
22. Y. P. Deng, X. H. Xie, H. Xiong, Y. X. Leng, C. F. Cheng, H. H. Lu, R. X. Li, and Z. Z. Xu, Opt. Express **13**, 3096 (2005).
23. G. J. Zhao, J. Y. Liu, L. C. Zhou, and K. L. Han, J. Phys. Chem. B **111**, 8940 (2007).
24. S. Woutersen, U. Emmerichs, and H. J. Bakker, J. Chem. Phys. **107**, 1483 (1997).